AD-A148 784 NUMERICAL COMPUTATION OF BASE FLOW FOR A MISSILE IN THE PRESENCE OF A CEN..(U) ARMY BALLISTIC RESEARCH LAB ABERDEEN PROVING GROUND MD J SAHU ET AL. OCT 84 1/1

UNCLASSIFIED BRL-MR-3397 SBI-AD-F300 510 F/G 20/4 NL

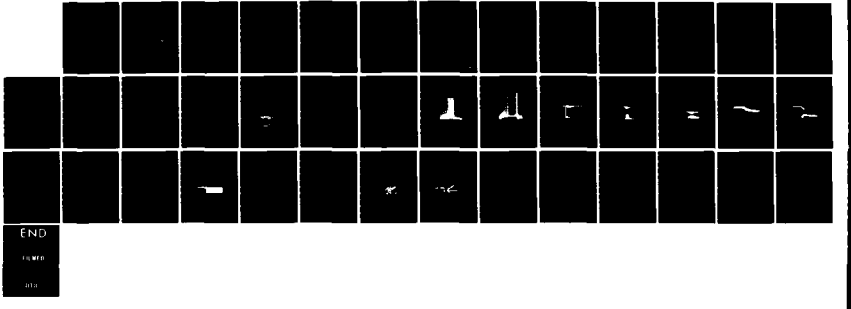

END

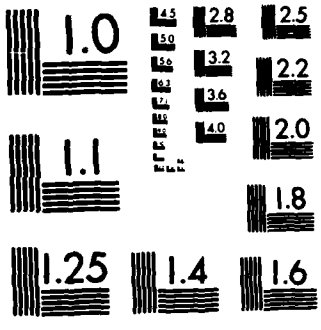

BRL

MEMORANDUM REPORT BRL-MR-3397

NUMERICAL COMPUTATION OF BASE FLOW FOR A MISSILE IN THE PRESENCE OF A CENTERED JET

Jubaraj Sahu
Charles J. Nietubicz

October 1984

US ARMY BALLISTIC RESEARCH LABORATORY
ABERDEEN PROVING GROUND, MARYLAND

Destroy this report when it is no longer needed.
Do not return it to the originator.

Additional copies of this report may be obtained from the National Technical Information Service, U. S. Department of Commerce, Springfield, Virginia 22161.

The findings in this report are not to be construed as an official Department of the Army position, unless so designated by other authorized documents.

The use of trade names or manufacturers' names in this report does not constitute indorsement of any commercial product.

UNCLASSIFIED

SECURITY CLASSIFICATION OF THIS PAGE (When Data Entered)

REPORT DOCUMENTATION PAGE		READ INSTRUCTIONS BEFORE COMPLETING FORM
1. REPORT NUMBER MEMORANDUM REPORT BRL-MR-3397	2. GOVT ACCESSION NO. AD-A148 784	3. RECIPIENT'S CATALOG NUMBER
4. TITLE (and Subtitle) NUMERICAL COMPUTATION OF BASE FLOW FOR A MISSILE IN THE PRESENCE OF A CENTERED JET		5. TYPE OF REPORT & PERIOD COVERED Final 6. PERFORMING ORG. REPORT NUMBER
7. AUTHOR(s) Jubaraj Sahu and Charles J. Nietubicz		8. CONTRACT OR GRANT NUMBER(s)
9. PERFORMING ORGANIZATION NAME AND ADDRESS U.S. Army Ballistic Research Laboratory ATTN: AMXBR-LFD Aberdeen Proving Ground, Maryland 21005-5066		10. PROGRAM ELEMENT, PROJECT, TASK AREA & WORK UNIT NUMBERS RDT&E 1L161102AH43
11. CONTROLLING OFFICE NAME AND ADDRESS U.S. Army Ballistic Research Laboratory ATTN: AMXBR-OD-ST Aberdeen Proving Ground, MD 21005-5066		12. REPORT DATE October 1984 13. NUMBER OF PAGES 41
14. MONITORING AGENCY NAME & ADDRESS(if different from Controlling Office)		15. SECURITY CLASS. (of this report) Unclassified 15a. DECLASSIFICATION/DOWNGRADING SCHEDULE

16. DISTRIBUTION STATEMENT (of this Report)

Approved for public release, distribution unlimited.

17. DISTRIBUTION STATEMENT (of the abstract entered in Block 20, if different from Report)

18. SUPPLEMENTARY NOTES

This report supersedes BRL IMR 789, dated September 1983.

19. KEY WORDS (Continue on reverse side if necessary and identify by block number)

Navier-Stokes Computations
Propulsive Jet
Implicit Algorithm
Axisymmetric Afterbody
Base Flow
Compressible
Time Dependent

20. ABSTRACT (Continue on reverse side if necessary and identify by block number)

A thin-layer Navier-Stokes base flow code, developed for projectile aerodynamics, has been used to compute the missile base flow in the presence of a centered propulsive jet. The thin-layer, compressible, Navier-Stokes equations are solved using a time dependent, implicit numerical algorithm. Numerical computations have been made to predict the missile afterbody flow field for both jet-off and jet-on conditions. Solutions are obtained for an axisymmetric cylindrical afterbody where the free stream Mach number is 1.343

DD FORM 1 JAN 73 1473 EDITION OF 1 NOV 65 IS OBSOLETE

UNCLASSIFIED

SECURITY CLASSIFICATION OF THIS PAGE (When Data Entered)

20. ABSTRACT (Continued)

and the jet exit Mach number is 2.7. The exhaust jet static pressure is 2.15 times the free stream static pressure. Computed results show both qualitative and quantitative features of the base region flow field.

TABLE OF CONTENTS

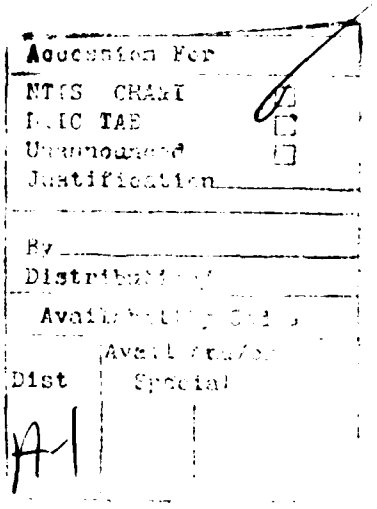

LIST OF ILLUSTRATIONS

I. INTRODUCTION

The aerodynamic drag associated with afterbody configurations is influenced both by the afterbody geometry and by the interaction of the exhaust jet with the external flow. The exhaust jet has a large influence on the base pressure and can influence the flow on the afterbody for large jet pressure. The flow field for such cases is complex due to strong viscous/inviscid interaction and regions of flow recirculation. Because of the strong interaction involved between flow regimes, it is advantageous to use the Navier-Stokes computational technique since it considers the interactions in a fully-coupled manner.

As part of a continued research effort at BRL, numerical computational capabilities have been developed to predict the aerodynamic behavior of artillery shell. References 1 and 2 have reported the development and application of the Azimuthal-Invariant Thin-Layer Navier-Stokes computational technique to predict the flow about slender bodies of revolution at transonic speeds. These calculations, however, did not include the base region flow field and modeled the wake as an extension of the afterbody. Recently, a new numerical capability[3,4] has been developed for the simulation of the complete projectile including the base region. This code has been used to predict the base pressure of shell at transonic speeds both with and without base bleed. The objective of the present research work was to use this base flow code and extend its capability to predict the effects of a centered propulsive jet on the base region flow field. The same numerical technique has been used by Deiwert[5] for a computational investigation of supersonic axisymmetric afterbodies containing a centered propulsive jet. However, his method of solution

---

1. *C. J. Nietubicz, T. H. Pulliam, and J. L. Steger, "Numerical Solution of the Azimuthal-Invariant Thin-Layer Navier-Stokes Equations," U.S. Army Ballistic Research Laboratory, Aberdeen Proving Ground, Maryland, ARBRL-TR-02227, March 1980. (AD A085716)*

2. *C. J. Nietubicz, "Navier-Stokes Computations for Conventional and Hollow Projectile Shapes at Transonic Velocities," U.S. Army Ballistic Research Laboratory, Aberdeen Proving Ground, Maryland, ARBRL-MR-03184, July 1982. (AD A116866)*

3. *J. Sahu, C. J. Nietubicz, and J. L. Steger, "Numerical Computation of Base Flow for a Projectile at Transonic Speeds," U.S. Army Ballistic Research Laboratory, Aberdeen Proving Ground, Maryland, ARBRL-TR-02495, June 1983. (AD A130293)*

4. *J. Sahu, C. J. Nietubicz, and J. L. Steger, "Navier-Stokes Computations of Projectile Base Flow with and without Base Injection," U.S. Army Ballistic Research Laboratory, Aberdeen Proving Ground, Maryland, ARBRL-TR-02532, November 1983. (AD A133684)*

5. *G. S. Deiwert, "A Computational Investigation of Supersonic Axisymmetric Flow Over Boattails Containing a Centered Propulsive Jet," AIAA Paper No. 83-0462, January 1983.*

and treatment of the computational mesh differs substantially from our current approach.

A brief description of the computational technique is given in Section II. A novel flow field segmentation procedure, equivalent to using multiple adjoining grids, is used and described in Section III. The model geometry and test conditions are given in Section IV and the generation of the computational grid is described in Section V. In Section VI, results are presented for afterbody flow field computations for both jet-off and jet-on conditions. The free stream Mach number is 1.343 and the jet exit Mach number is 2.7. The exhaust jet static pressure is 2.15 times the free stream pressure and the conical nozzle half angle is 10°. The Reynolds number of the external flow based on maximum body diameter is 0.92×10^6. These computations correspond to the experiments conducted by Walker[6] for the same configuration and flow conditions. The fluid has been assumed to be air in both the external flow and the exhaust, although nitrogen was used in the exhaust in the actual experiments.

II. COMPUTATIONAL TECHNIQUE

The Azimuthal Invariant (or Generalized Axisymmetric) thin-layer Navier-Stokes equations for general spatial coordinates ξ, η, ζ can be written as[2]

$$\partial_\tau \hat{q} + \partial_\xi \hat{E} + \partial_\zeta \hat{G} + \hat{H} = Re^{-1} \partial_\zeta \hat{S} \tag{1}$$

where $\xi = \xi(x,y,z,t)$ is the longitudinal coordinate

$\eta = \eta(y,z,t)$ is the circumferential coordinate

$\zeta = \zeta(x,y,z,t)$ is the near normal coordinate

$\tau = t$ is the time

and

$$\hat{q} = J^{-1} \begin{bmatrix} \rho \\ \rho u \\ \rho v \\ \rho w \\ e \end{bmatrix}, \quad \hat{E} = J^{-1} \begin{bmatrix} \rho U \\ \rho uU + \xi_x p \\ \rho vU + \xi_y p \\ \rho wU + \xi_z p \\ (e+p)U - \xi_t p \end{bmatrix}, \quad \hat{G} = J^{-1} \begin{bmatrix} \rho W \\ \rho uW + \zeta_x p \\ \rho vW + \zeta_y p \\ \rho wW + \zeta_z p \\ (e+p)W - \zeta_t p \end{bmatrix}$$

---

6. *B. J. Walker, "Tactical Mission Base Flow," Paper presented at Symposium on Rocket/Plume Fluid Dynamic Interactions, Huntsville, Alabama, April 1983.*

$$\hat{H} = J^{-1} \begin{bmatrix} 0 \\ 0 \\ \rho V[R_\xi(U-\xi_t) + R_\zeta(W-\zeta_t)] \\ -\rho VR(V-\eta_t) - p/R \\ 0 \end{bmatrix}$$

$$\hat{S} = \begin{bmatrix} 0 \\ \mu(\zeta_x^2 + \zeta_y^2 + \zeta_z^2)u_\zeta + (\mu/3)(\zeta_x u_\zeta + \zeta_y v_\zeta + \zeta_z w_\zeta)\zeta_x \\ \mu(\zeta_x^2 + \zeta_y^2 + \zeta_z^2)v_\zeta + (\mu/3)(\zeta_x u_\zeta + \zeta_y v_\zeta + \zeta_z w_\zeta)\zeta_y \\ \mu(\zeta_x^2 + \zeta_y^2 + \zeta_z^2)w_\zeta + (\mu/3)(\zeta_x u_\zeta + \zeta_y v_\zeta + \zeta_z w_\zeta)\zeta_z \\ \{(\zeta_x^2 + \zeta_y^2 + \zeta_z^2)[(\mu/2)(u^2 + v^2 + w^2)_\zeta + \kappa Pr^{-1}(\gamma - 1)^{-1}(a^2)_z] \\ \quad + (\mu/3)(\zeta_x u + \zeta_y v + \zeta_z w)(\zeta_x u_\zeta + \zeta_y v_\zeta + \zeta_z w_\zeta)\} \end{bmatrix}$$

The velocities

$$\begin{aligned} U &= \xi_t + \xi_x u + \xi_y v + \xi_z w \\ V &= \eta_t + \eta_x u + \eta_y v + \eta_z w \\ W &= \zeta_t + \zeta_x u + \zeta_y v + \zeta_z w \end{aligned} \tag{2}$$

represent the contravariant velocity components.

The Cartesian velocity components (u, v, w) are nondimensionalized with respect to a_∞ (free stream speed of sound). The density (ρ) is referenced to ρ_∞ and total energy (e) to $\rho_\infty a_\infty^2$. The local pressure is determined using the equation of state,

$$P = (\gamma - 1)[e - 0.5\rho(u^2 + v^2 + w^2)] \tag{3}$$

where γ is the ratio of specific heats.

In Equation (1), axisymmetric flow assumptions have been made which result in the source term, $\hat{H}$. The details of how this is obtained can be found in Reference 2 and are not discussed here. Equation (1) contains only two spatial derivatives. However, it retains all three momentum equations and

allows a degree of generality over the standard axisymmetric equations. In particular, the circumferential velocity is not assumed to be zero, thus allowing computations for spinning projectiles to be accomplished.

The numerical algorithm used is the Beam-Warming fully implicit, approximately factored finite difference scheme. The algorithm can be first or second order accurate in time and second or fourth order accurate in space. Since the interest is only in the steady-state solution, Equation (1) is solved in a time asympotic fashion and first order accurate time differencing is used. The spatial accuracy is fourth order. Details of the algorithm are included in References 7-9.

For the computation of turbulent flows, a turbulence model must be supplied. In the present calculations a two layer algebraic eddy viscosity model by Baldwin and Lomax[10] is used. In their two layer model the inner region follows the Prandtl-Van Driest formulation. Their outer formulation can be used in wakes as well as in attached and separated boundary layers. In both the inner and outer formulations, the distribution of vorticity is used to determine length scales, thereby avoiding the necessity of finding the outer edge of the boundary layer (or wake). The magnitude of the local vorticity for the axisymmetric formulation is given by

$$|\omega| = \sqrt{\left(\frac{\partial v}{\partial x}\right)^2 + \left(\frac{\partial v}{\partial z} - \frac{\partial w}{\partial y}\right)^2 + \left(\frac{\partial w}{\partial x} - \frac{\partial u}{\partial z}\right)^2} \quad . \tag{4}$$

In determining the outer length scale a function[10]

$$F(y) = y|\omega| \left[1 - \exp(-y^+/A^+)\right] \tag{5}$$

---

7. *J. L. Steger, "Implicit Finite Difference Simulation of Flow About Arbitrary Geometries with Application to Airfoils," AIAA Journal, Vol. 16, No. 7, July 1978, pp. 679-686.*

8. *T. H. Pulliam, and J. L. Steger, "On Implicit Finite-Difference Simulations of Three-Dimensional Flow," AIAA Journal, Vol. 18, No. 2, February 1980, pp. 159-167.*

9. *R. Beam, and R. F. Warming, "An Implicit Factored Scheme for the Compressible Navier-Stokes Equations," AIAA Journal, Vol. 16, No. 4, April 1978, pp. 393-402.*

10. *B. S. Baldwin, and H. Lomax, "Thin-Layer Approximation and Algebraic Model for Separated Turbulent Flows," AIAA Paper No. 78-257, 1978.*

is used where y^+ and A^+ are the conventional boundary layer terms. For the base flow (or wake flow) the exponential term of Equation (5) is set equal to zero.

III. METHOD OF SOLUTION

A. Base Region Flow with Jet-Off

The procedure used to compute the base flow without jet for projectile configuration has been described in Reference 3; however, limited details will be repeated here for clarity. The code computes the full flow field (including the base region) of a projectile. Figure 1 shows a schematic illustration of the flow field segmentation used in this study for computational purposes. It shows the transformation of the physical domain into the computational domain and the details of the flow field segmentation procedure in both domains. This flow field segmentation procedure is equivalent to using multiple adjoining grids. An important advantage of this procedure lies in the preservation of the sharp corner at the base and allows easy blending of the computational meshes between the regions ABCD and AEFG. No approximation of the actual sharp corner at the base is made. Thus, realistic representation of the base is inherent in the current procedure.

The cross hatched region represents the model. The line BC is the base and the region ABCD is the base region or the wake. The line AB is a computational cut through the physical wake region which acts as a repetitive boundary in the computational domain. Implicit integration is carried out in both ξ and ζ directions (see Figure 1). Note the presence of the lines BC (base) and EF (nose axis) in the computational domain. They both act as boundaries in the computational domain and special care must be taken in inverting the block tridiagonal matrix in the ξ direction. The details of these can be found in References 3 and 4 and are not included here.

The no slip boundary condition for viscous flow is enforced by setting

$$U = V = W = 0 \tag{6}$$

on the body surface. At the base boundary, inviscid boundary condition has been used. Additionally, at the corner of the base, the boundary conditions are double-valued and depend on the direction from which the corner is approached. Approaching it in the streamwise direction (EB), the no-slip boundary condition is used; while approaching in the radial direction (along the base, CB), inviscid boundary condition is used. Along the computational cut (AB), the flow variables above and below the cut are simply averaged to determine the boundary conditions on the cut. On the centerline of the wake region, a symmetry condition is imposed and free stream conditions are used on the outer boundary. First order extrapolation for all flow variables is used at the downstream boundary.

B. Base Region Flow with Jet-On

The method of solution for the case with a centered propulsive jet remains essentially the same as described in Section III A. The boundary conditions on the body surface, the cut, and the downstream boundary also remain the same as previously described. Along that part of the base boundary which does not contain the nozzle, same conditions described earlier are used. For the remaining part of the base boundary (i.e., the nozzle exit), boundary conditions are used based on the nozzle exit Mach number, stagnation temperature, and pressure. The velocity components are linearly interpolated from the center line of symmetry to the nozzle height at the exit i.e., conical flow at the jet exit has been assumed.

IV. MODEL AND TEST CONDITIONS

The model geometry used in this study is shown in Figure 2. It consists of a 4 caliber tangent-ogive nose and a 5 caliber cylindrical afterbody. The base diameter is 1 caliber and the nozzle exit diameter is 0.2 caliber.

The experimental model was side-wall mounted in AEDC Wind Tunnel[6] 1-T as shown in Figure 2a; additional details of the nozzle and base are shown in Figure 2b. The wind tunnel and nozzle test conditions are summarized below.

Free Stream Flow

Gas: Air
Stagnation Temperature: 190°F
Static Pressure: 6.14 psia
Free Stream Mach Number: 1.343

Nozzle Flow

Gas: Nitrogen
Stagnation Temperature: 207°F
Stagnation Pressure: 307.7 psia
Exit Design Mach Number: 2.7

Detailed experimental measurements of the base region flow field have been made by Walker.[6] The data were obtained using a two-component LDV system. Figure 3 is a sketch of the aft end of the model and shows the regions for which the data is presented. The test results have not been released. A "sealed envelope" comparison between computational models and experimental results for the MICOM model with a centered propulsive jet is being carried out by the U.S. Army Missile Command. Various groups are performing computations and MICOM will make the comparison. At this point, limited experimental data is available in the form of velocity components and Mach number at two boundary stations (see Figure 4). The available experimental data at a station 1.6 caliber upstream of the base has been used as an upstream boundary condition in some of the numerical calculations. The fluid has been assumed to be air for bothfree stream and nozzle flows in the present computations.

V. COMPUTATIONAL GRID

Figure 5 shows the computational grid used for the numerical computations. This grid was obtained in two segments consistent with the flow field segmentation procedure described earlier in Section III A. The first segment of the computational mesh is for region AEFG (see Figure 1) and was obtained from a grid generation program developed by Steger et al.[11] The grid for the second segment, region ABCD, was obtained by another procedure to be described later in this section. The grid generation program by Steger et al[11] allows arbitrary grid point clustering, thus enabling grid points for the projectiles to be clustered in the vicinity of the body surface. The grid consists of 109 points in the longitudinal direction with 25 points in the base region and 40 points in the radial direction. The computational domain extended to little more than a body length in front, about 3 body lengths in the radial direction and about 2 body lengths behind the base of the missile. The grid points in the normal direction were exponentially stretched away from the surface with a minimum spacing at the wall of .00002D. This spacing locates at least two points within the laminar sublayer.

An expanded view of the grid in the vicinity of the model is shown in Figure 6. As stated earlier, the grid shown in Figures 5 and 6 was generated in two segments. First, the grid in the outer region AEFG is obtained using an elliptic solver[11] for the ogive portion. Straight-line rays are used for the remaining portion which runs all the way to the downstream boundary. Second, the grid in the base region ABCD is obtained simply by extending the straight lines perpendicular to line AB down to the line of symmetry (line CD). In other words, same grid stretching is used in the longitudinal direction in both the regions above and below the line AB. It remains then to generate the grid spacings in the normal direction in the base region ABCD. For base flow computations with a centered propulsive jet, it is desirable to cluster grid points near the cut to resolve the flow gradients in the shear layer as well as near the line of symmetry where jet is present. A 1-D elliptic equation solver was used to generate the grid spacings in the normal direction in the base region ABCD. This technique enables the desired minimum spacing to be specified at both ends. It should be noted that the same minimum spacing .00002D is specified on both sides of the cut thus maintaining a smooth variation of grid across the cut. This spacing could, of course, be increased downstream of the base. The number of grid points above and below line AB is the same (40 points). As can be seen in Figure 6, the grid points are clustered near the nose-cylinder junction and at the projectile base where appreciable changes in flow variables are expected.

When computations over the entire model are made, only a limited number of grid points can be used in the base region. One way to eliminate this restriction is to use known data given by experiment or otherwise at a station upstream of the base and then compute the flow field in the isolated base

---

11. J. L. Steger, C. J. Nietubicz, and K. R. Heavey, "A General Curvilinear Grid Generation Program for Projectile Configurations," U.S. Army Ballistic Research Laboratory, Aberdeen Proving Ground, Maryland, ARBRL-MR-03142, October 1981. (AD A107334)

region only. This, of course, allows a large number of grid points to be used in the base region and can be used to determine grid dependancy on the computed solution in the base region. This capability was initially developed by the current authors for the numerical computations of base region flow field at supersonic velocities. Solutions were obtained for a cone-cylinder configuration with the space-marching PNS (Parabolized Navier-Stokes) code. This generated a solution at a station upstream of the base, and this solution was then used as the upstream boundary condition for the computation of the base region flow field by the unsteady base flow code. In the present computations, experimental data is known at a station upstream of the base, and is thus used as the upstream boundary condition in the numerical computations when full grid is not used.

VI. RESULTS

Results are now presented for both jet-off and jet-on cases. Figure 7 shows the velocity vectors in the base region when there is no jet present. Each vector shows the magnitude and direction of the velocity at that point. The recirculatory flow in the base region is clearly evident. Figure 8 shows the effect of the centered jet on the near wake flow field. The near wake flow field has changed considerably and the recirculation region has been reduced. This figure has been stretched in the vertical direction to show the qualitative features as clearly as possible. A scaled result is shown in Figure 9, and is a more realistic representation of the near wake flow field with jet-on.

Figures 10 and 11 show the stream function contours in the base region. Figure 10 is for the jet-off case and clearly shows the separation bubble. The reattachment point is about two calibers down from the base. The effect of the jet is shown in Figure 11. The separation bubble has been considerably reduced in size.

Quantitatively, one is interested in how the complex flow field in the base region affects the base pressure. Figure 12 shows the variation of base pressure along the base for jet-off conditions. When there is no jet present, base pressure is high near the corner of the base. It decreases gradually and then recovers to almost the free stream static pressure near the center line of symmetry. This variation of base pressure along the base is substantiated by other experimental observations.[12] The cone model for the experimental measurements of Reference 12 is shown in Figure 13a. The model was supported by a sting attached to the base. Figure 13b shows the typical base pressure variation along the base for various Reynolds numbers and $M_\infty = 1.75$. There is some effect of the sting on these variations; however, the experimental base pressure profiles have the same qualitative variations as predicted by the present computations (Figure 12).

---

12. *L. D. Kayser, "Experimental Study of Separation from the Base of a Cone at Supersonic Speeds," U.S. Army Ballistic Research Laboratory, Aberdeen Proving Ground, Maryland, BRL Report No. 1737, August 1974. (AD A005015)*

The primary objective of this research was to compute the base flow in the presence of a centered propulsive jet. For the jet-on computations, the full grid shown in Figure 6 was used. Additionally, to determine grid dependancy on the solution, a large number of grid points were used in the base region and solutions were obtained for another grid shown in Figure 14. In this case, calculations were not performed on the full model. The given experimental data was used as an upstream boundary condition and computations were made for the isolated base region only. This allowed a large number of grid points to be used in the base region. The results of jet-on calculations for both grids are shown in Figure 15. Both of these jet-on calculations give practically the same base pressure variation along the base. At the nozzle exit plane, the base pressure shown is the specified jet pressure. For the remaining portion of the base, the effect of the jet has been to reduce the base pressure. The small oscillations in the base pressure distribution along the base are located near the two corners: one at the base, and the other formed by the base boundary and the nozzle. These oscillations are not physical and are believed to be due to the numerical difficulties associated with the boundary conditions at these corners. The base pressure distribution in general however, is a realistic representation associated with the base region flow field.

Additional qualitative features of the base region flow field are shown in Figures 16, 17 and 18 for the refined grid. Figure 16 shows the pressure distribution along the surface of the model and at Z/D = .5 downstream of the base corner as a function of axial position. The pressure distribution shows the rapid expansion which occurs at the base corner and the recompression that occurs downstream of the base. Figure 17 is a pressure contour plot in the wake region and clearly shows the expansion at the base and recompression shock downstream of the base. Figure 18 shows the Mach contours in the near wake flow field. The strong shear layer as well as the jet boundary in the base region are apparent. It also seems to indicate the presence of a Mach disk at X/D ≈ 9.75. The grid spacings in that vicinity are however, not as fine. Thus, a sharp picture of the Mach disk is not seen.

VII. SUMMARY

A recently developed numerical capability has been used to compute the missile base flow in the presence of a centered propulsive jet. The thin-layer, compressible, Navier-Stokes equations are solved using a time-dependent, implicit numerical algorithm.

Numerical computations have been made to predict the flow field over a missile afterbody for both jet-off and jet-on conditions. The free stream Mach number is 1.343 and the jet exit Mach number is 2.7. The exhaust jet static pressure is 2.15 times the free stream pressure and the conical nozzle half angle is 10°. Qualitative features of the near wake flow field have been shown in the form of velocity vector and contour plots of stream function, Mach number and pressure. Quantitatively, the effect of the jet has been shown to reduce the base pressure.

The experimental results are not available pending a sealed envelope comparison with computations by various groups. Comparison with the experimental measurements for the same model and same conditions will be made by MICOM.

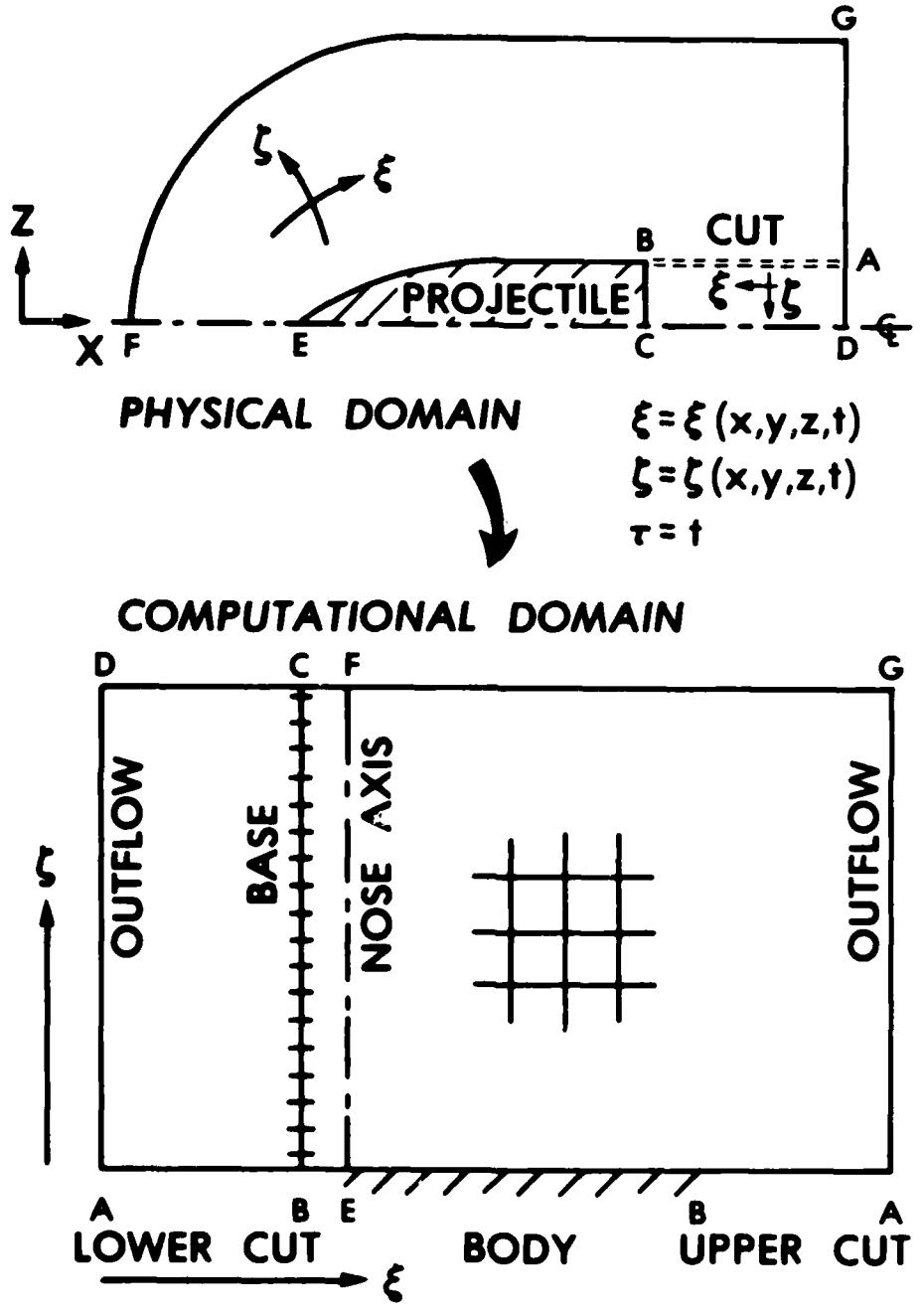

Figure 1. Schematic Illustration of Flow Field Segmentation

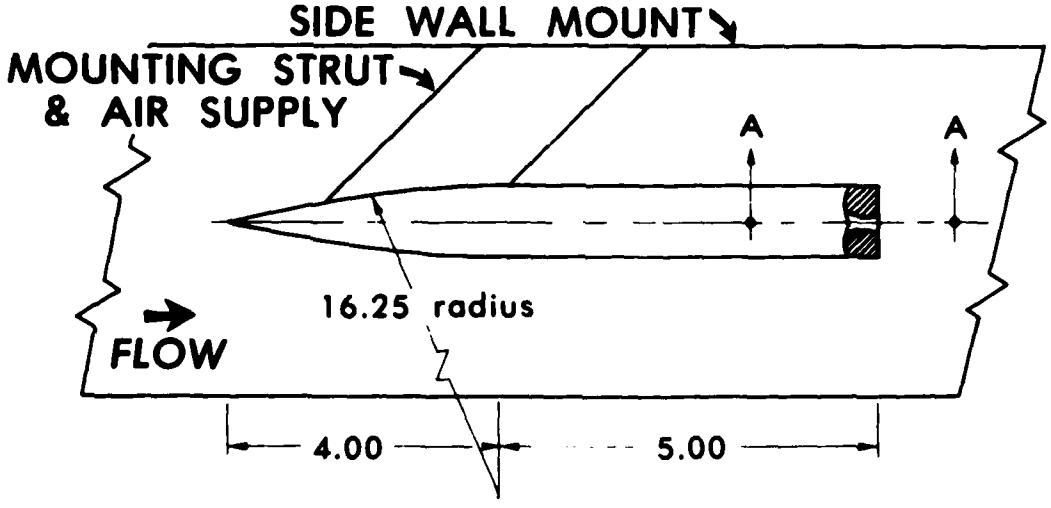

DIMENSIONS IN calibers
1 caliber = 63.5 mm (2.5 in)

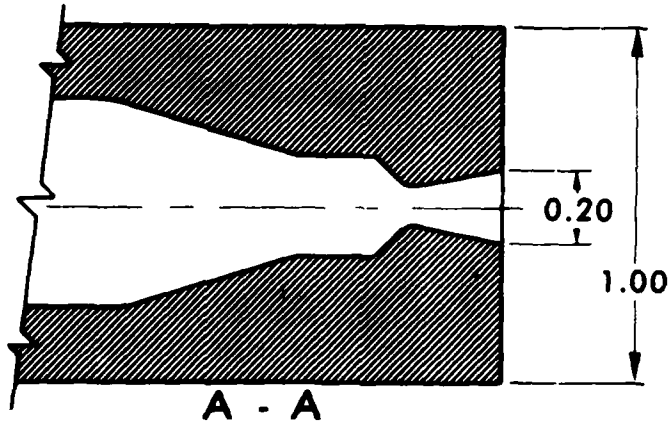

Figure 2. MICOM Base-Flow Model Mounted in the Wind Tunnel

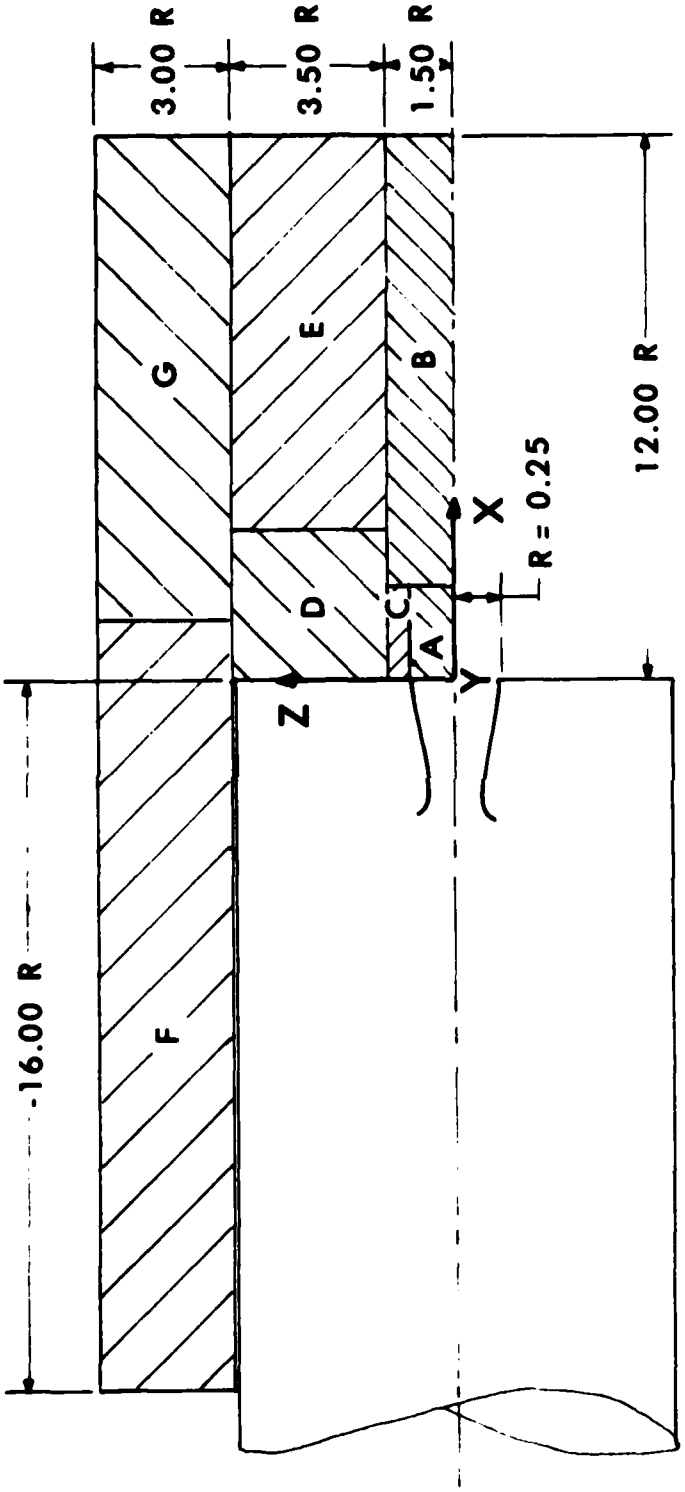

Figure 3. Base Flow Field Measurement Regions

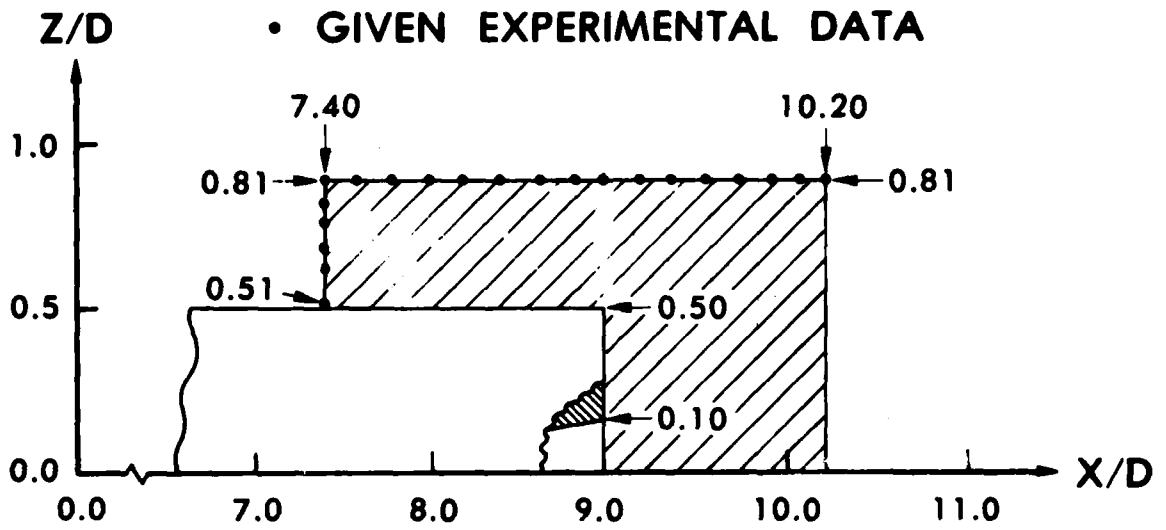

Figure 4. Configuration and Notation for the Experimentally Determined Boundary Data

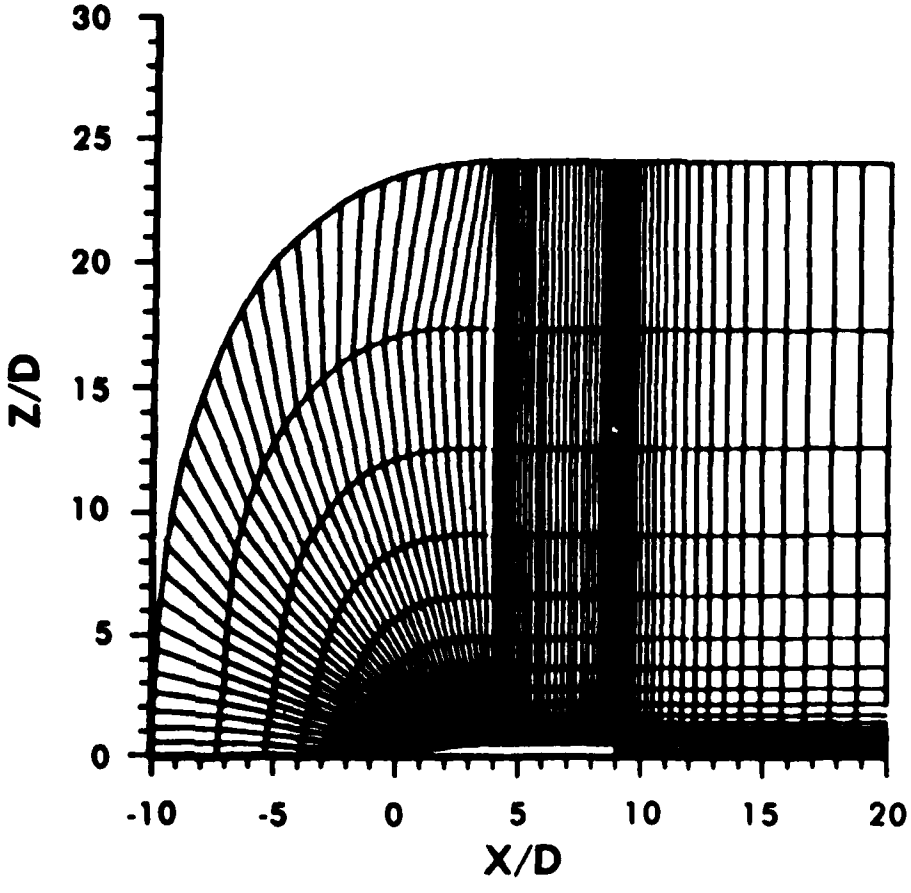

Figure 5. Computational Grid

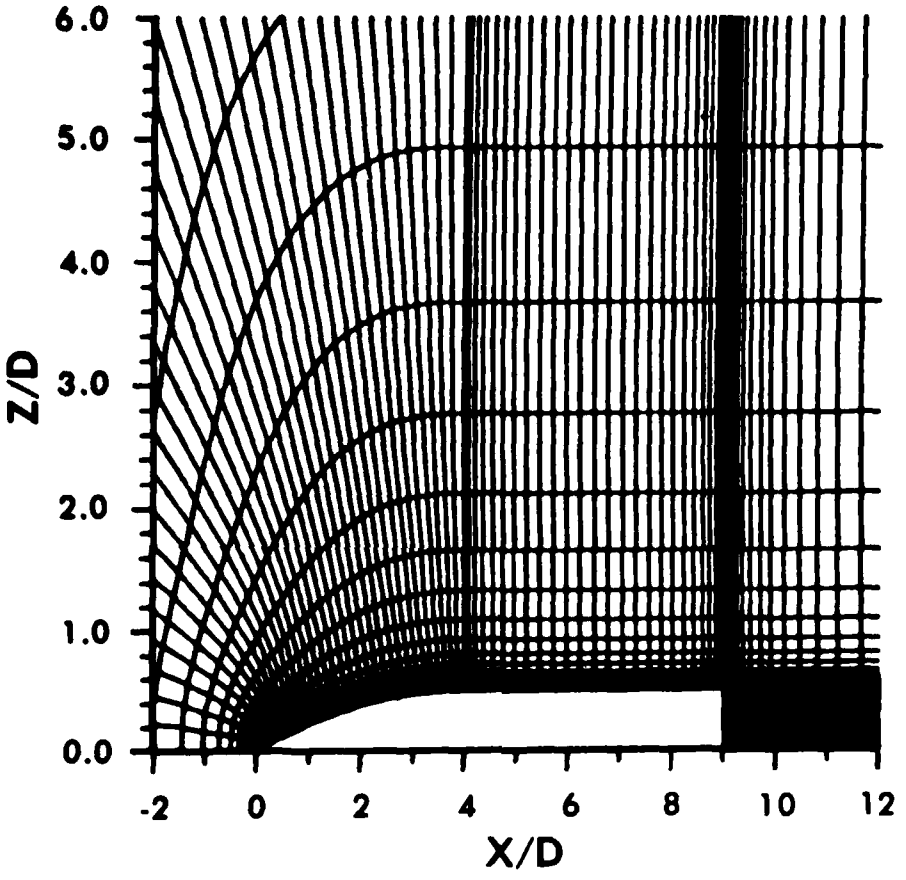

Figure 6. Expanded View of the Grid Near the Model

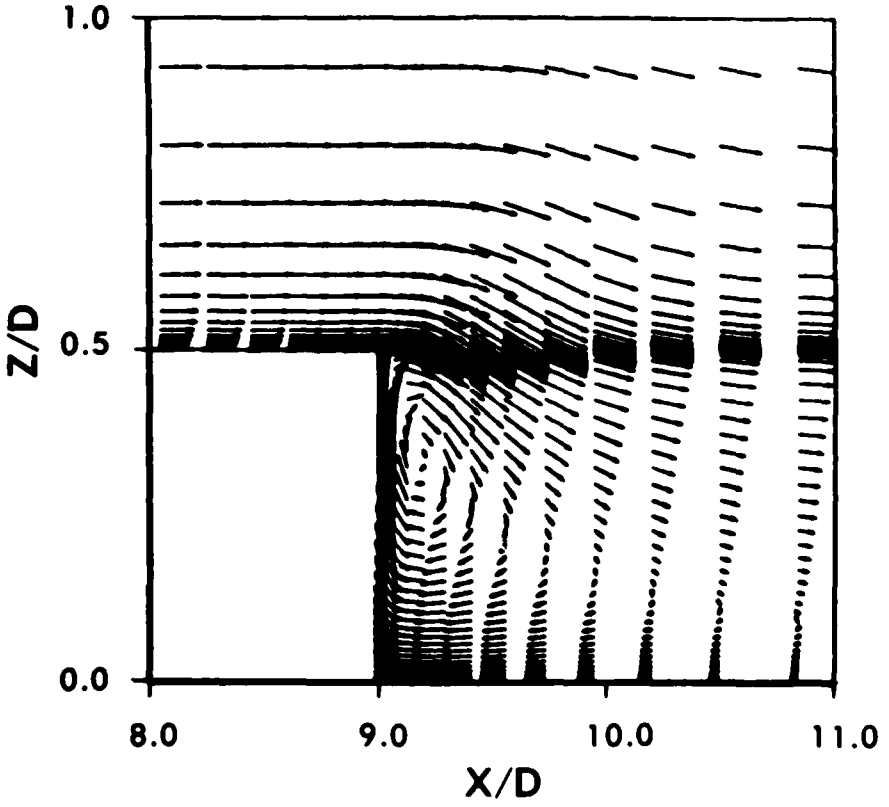

Figure 7. Velocity Vectors, M_∞ = 1.343, α = 0, Jet-Off

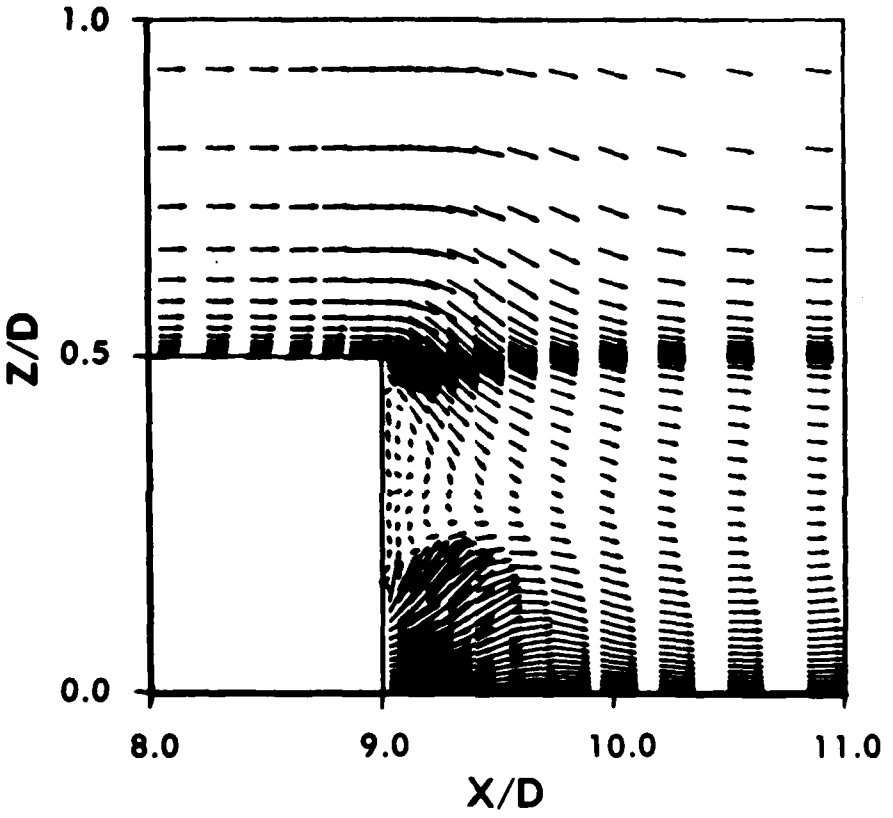

Figure 8. Velocity Vectors, M_∞ = 1.343, α = 0, Jet-On

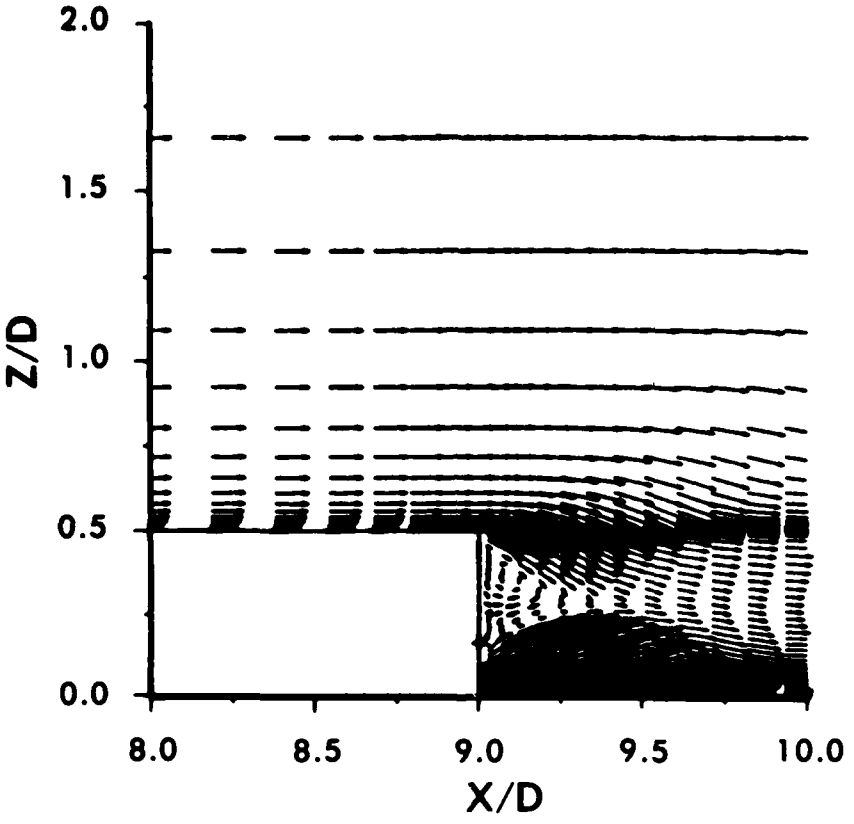

Figure 9. Velocity Vectors with Model Drawn to Scale, $M_\infty = 1.343$, $\alpha = 0$, Jet-On

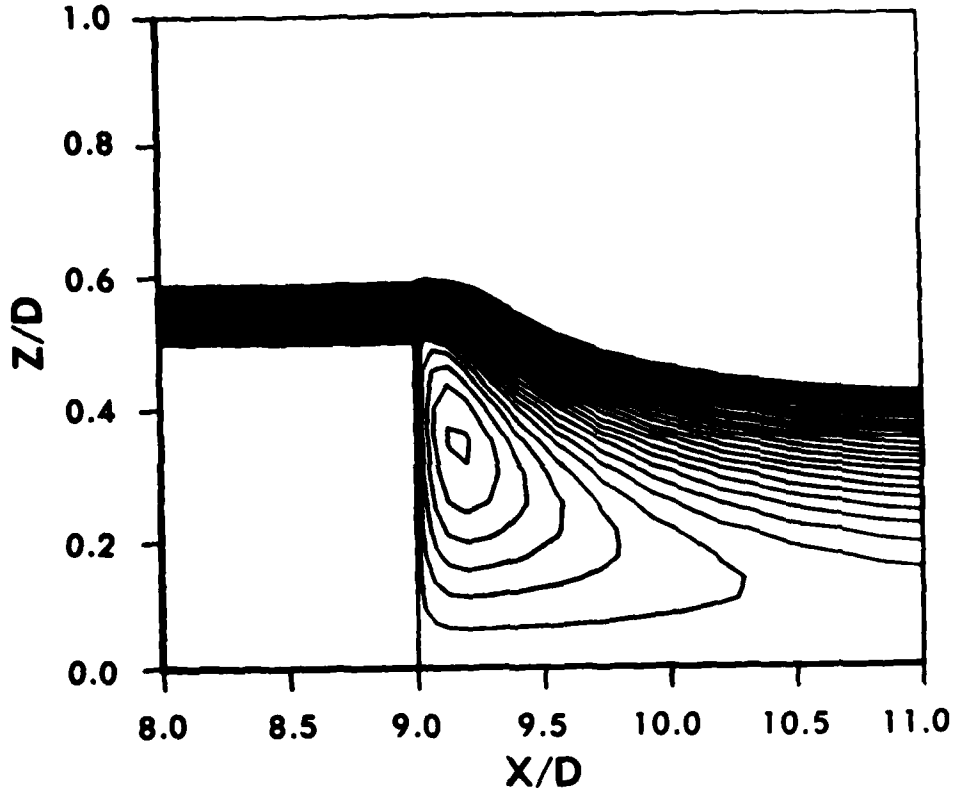

Figure 10. Stream Function Contours, M_∞ = 1.343, α = 0, Jet-Off

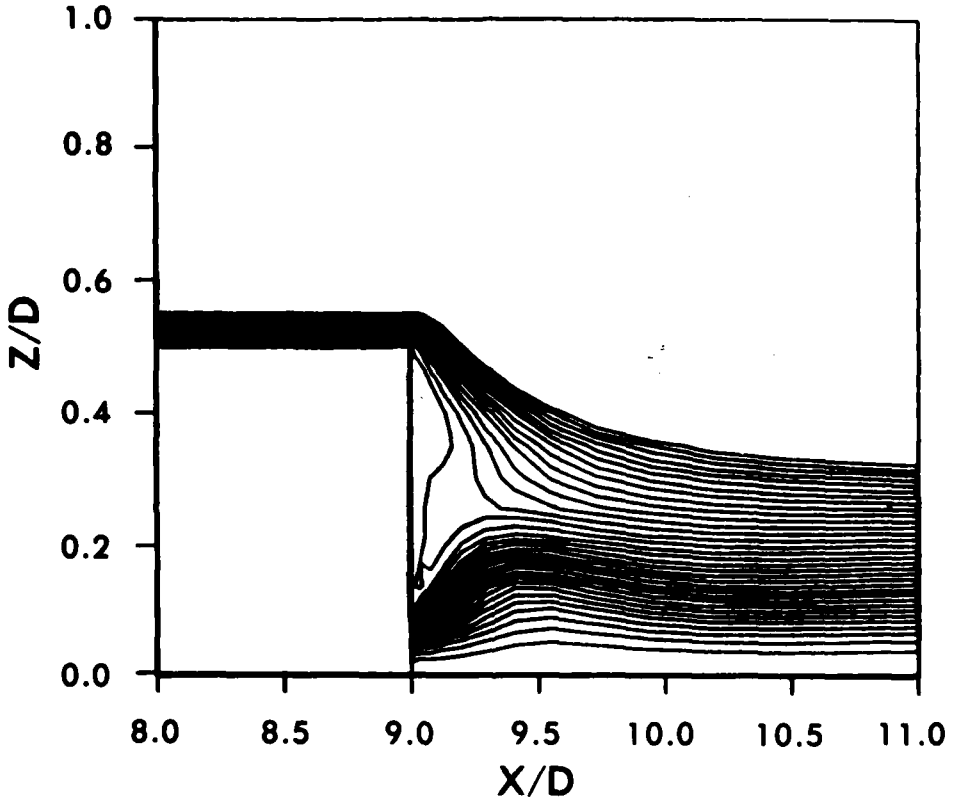

Figure 11. Stream Function Contours, M_∞ = 1.343, α = 0, Jet-On

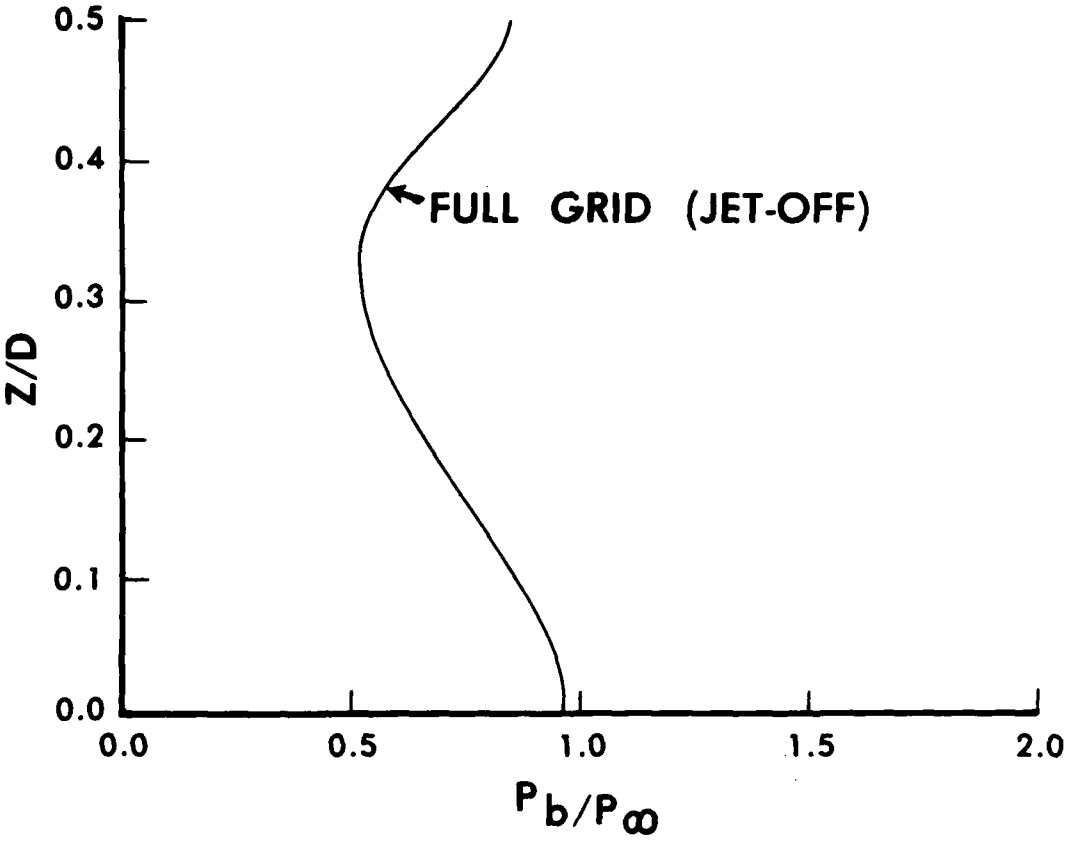

Figure 12. Variation of Base Pressure Along the Base, $M_\infty = 1.343$, $\alpha = 0$, Jet-Off

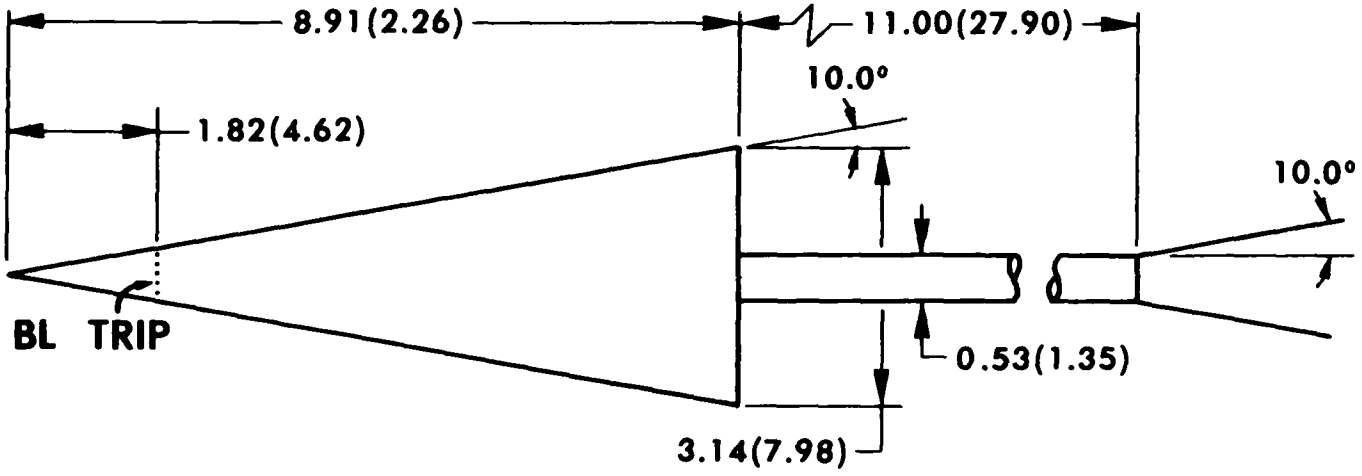

Figure 13a. Cone Wind Tunnel Model

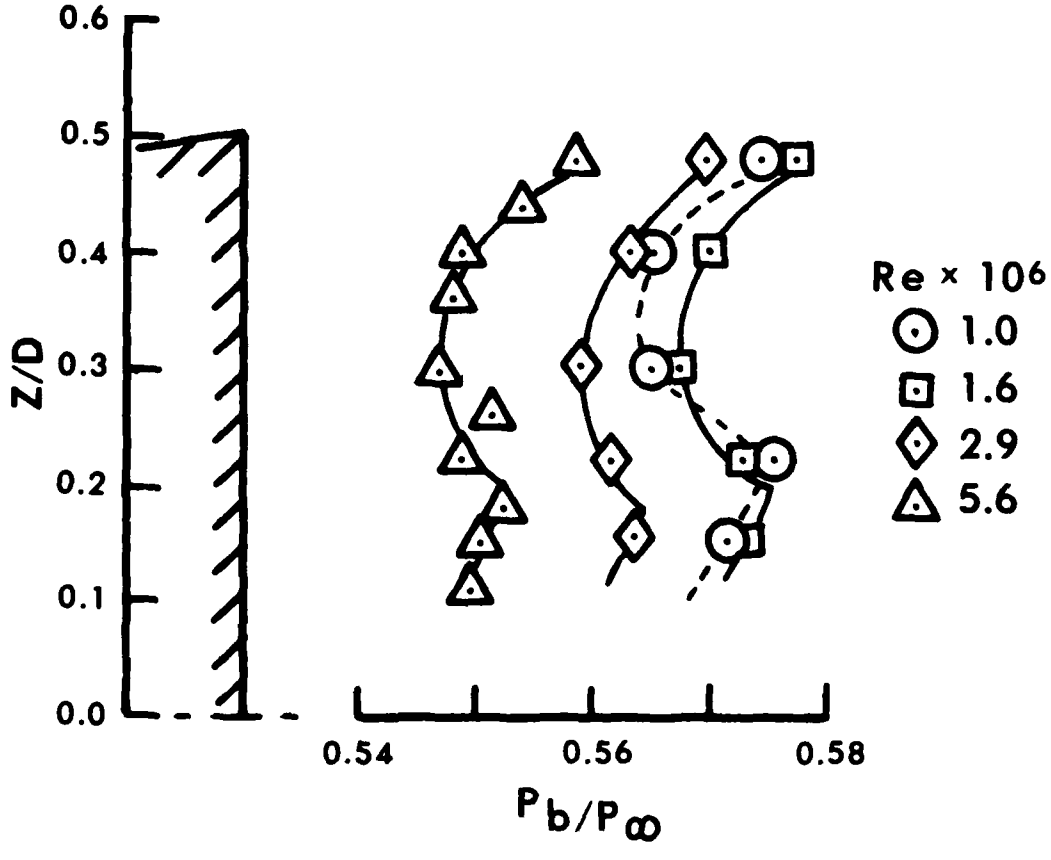

Figure 13b. Base Pressure Distribution for Cone

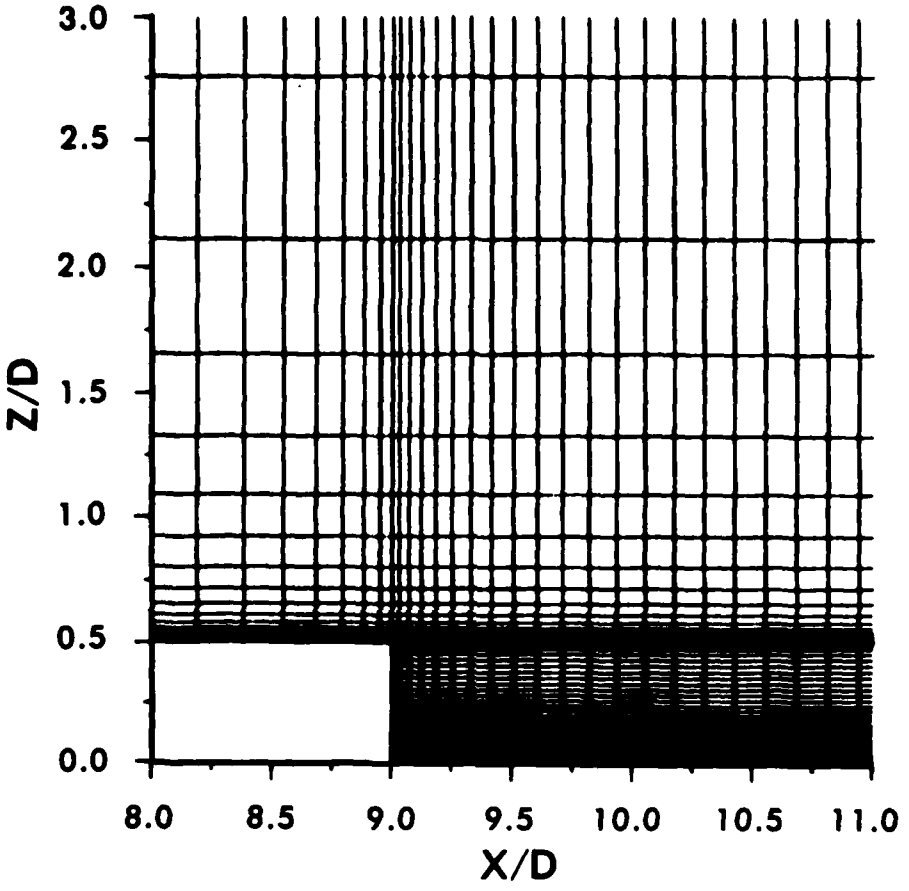

Figure 14. Expanded Grid for the Isolated Base Region Flow Field Computations

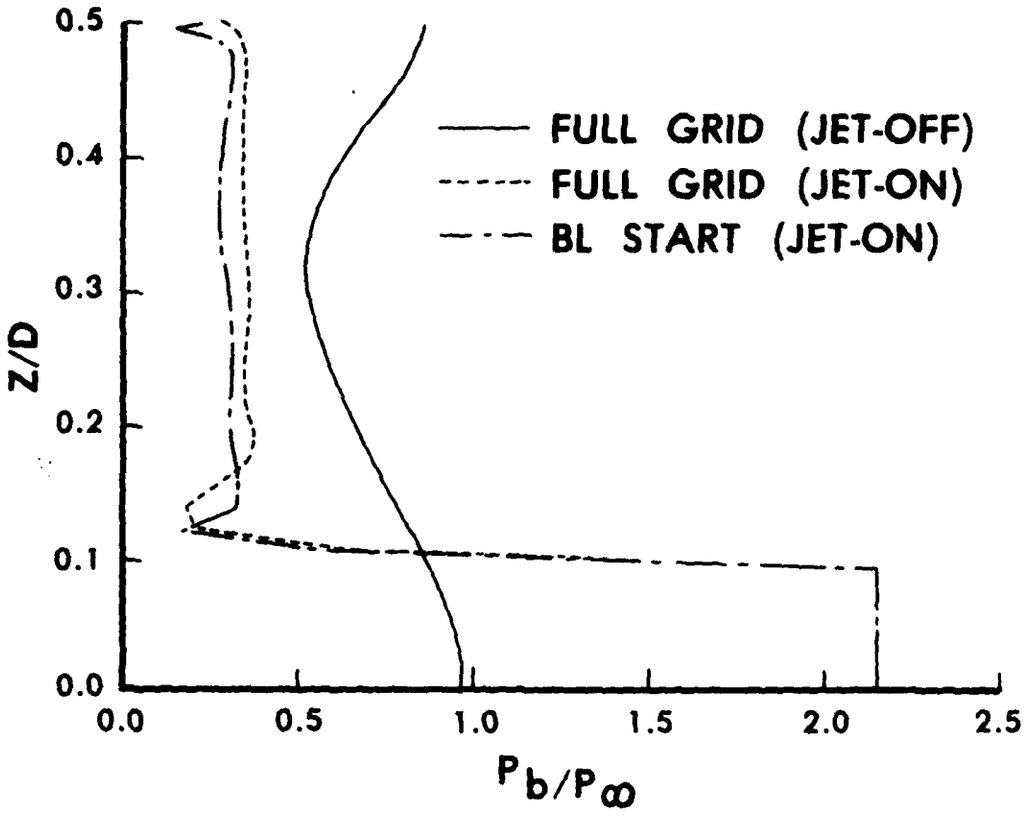

Figure 15. Variation of Base Pressure along the Base, $M_\infty = 1.343$, $\alpha = 0$, Jet-Off and Jet-On

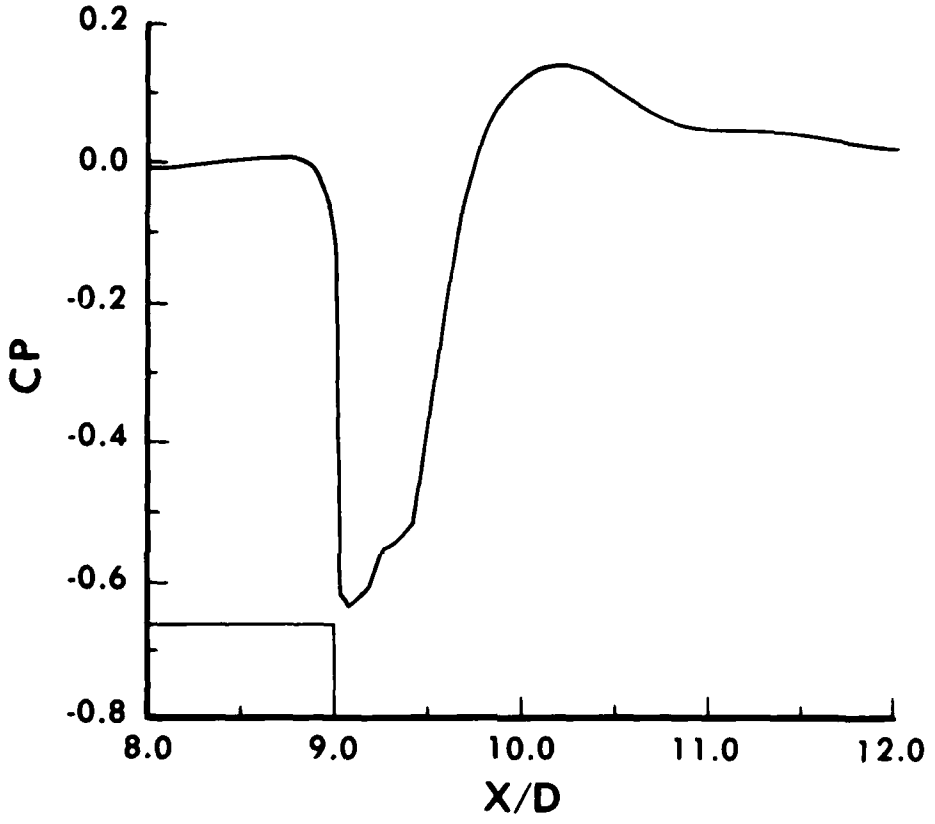

Figure 16. Static Pressure Distribution at Z/D = .5, M_∞ = 1.343, α = 0, Jet-On

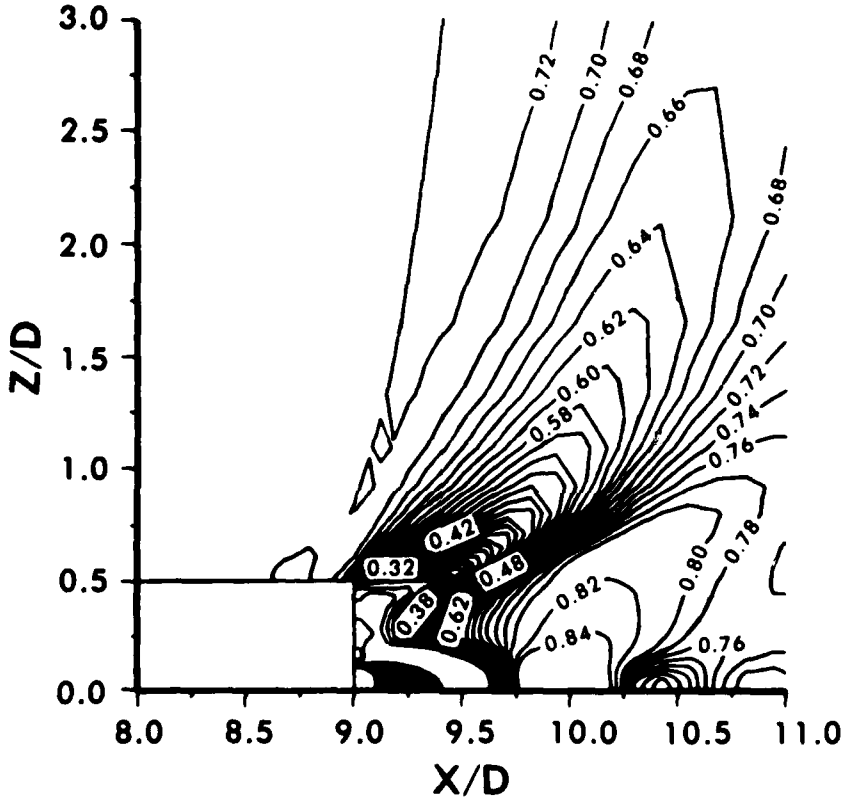

Figure 17. Pressure Contours, M_∞ = 1.343, α = 0, Jet-On

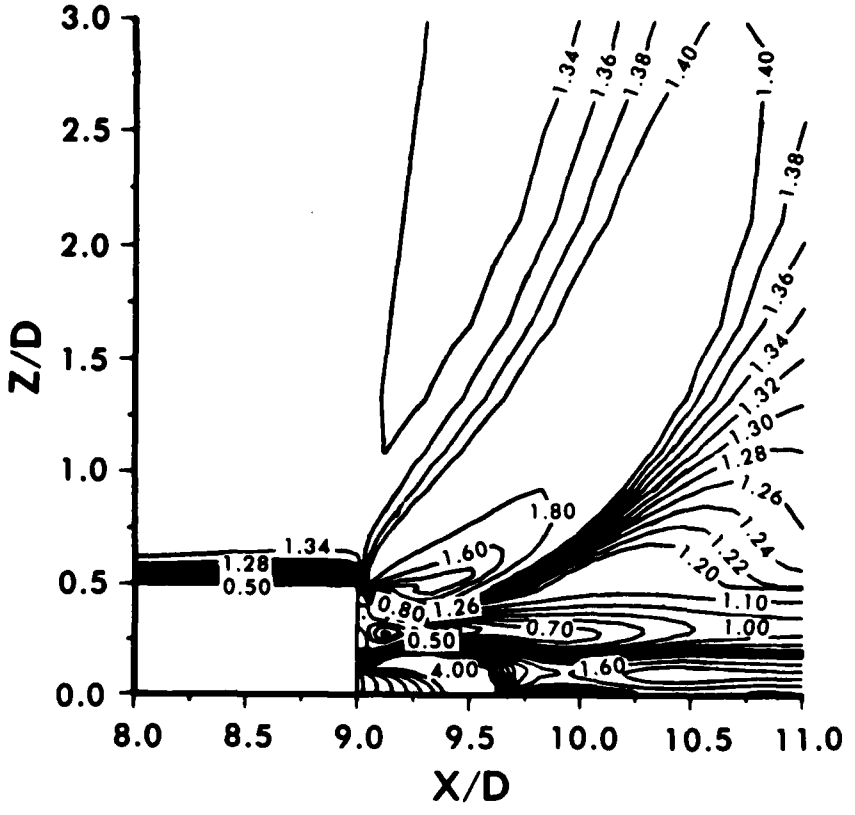

Figure 18. Mach Contours, M_∞ = 1.343, α = 0, Jet-On

REFERENCES

1. C. J. Nietubicz, T. H. Pulliam, and J. L. Steger, "Numerical Solution of the Azimuthal-Invariant Thin-Layer Navier-Stokes Equations," U.S. Army Ballistic Research Laboratory, Aberdeen Proving Ground, Maryland, ARBRL-TR-02227, March 1980. (AD A085716)

2. C. J. Nietubicz, "Navier-Stokes Computations for Conventional and Hollow Projectile Shapes at Transonic Velocities," U.S. Army Ballistic Research Laboratory, Aberdeen Proving Ground, Maryland, ARBRL-MR-03184, July 1982. (AD A116866)

3. J. Sahu, C. J. Nietubicz, and J. L. Steger, "Numerical Computation of Base Flow for a Projectile at Transonic Speeds," U.S. Army Ballistic Research Laboratory, Aberdeen Proving Ground, Maryland, ARBRL-TR-02495, June 1983. (AD A130293)

4. J. Sahu, C. J. Nietubicz, and J. L. Steger, "Navier-Stokes Computations of Projectile Base Flow with and without Base Injection," U.S. Army Ballistic Research Laboratory, Aberdeen Proving Ground, Maryland, ARBRL-TR-02532, November 1983. (AD A133684)

5. G. S. Deiwert, "A Computational Investigation of Supersonic Axisymmetric Flow Over Boattails Containing a Centered Propulsive Jet," AIAA Paper No. 83-0462, January 1983.

6. B. J. Walker, "Tactical Missile Base Flow," Paper presented at Symposium on Rocket/Plume Fluid Dynamic Interactions, Huntsville, Alabama, April 1983.

7. J. L. Steger, "Implicit Finite Difference Simulation of Flow About Arbitrary Geometries with Application to Airfoils," AIAA Journal, Vol. 16, No. 7, July 1978, pp. 679-686.

8. T. H. Pulliam, and J. L. Steger, "On Implicit Finite-Difference Simulations of Three-Dimensional Flow," AIAA Journal, Vol. 18, No. 2, February 1980, pp. 159-167.

9. R. Beam, and R. F. Warming, "An Implicit Factored Scheme for the Compressible Navier-Stokes Equations," AIAA Journal, Vol. 16, No. 4, April 1978, pp. 393-402.

10. B. S. Baldwin, and H. Lomax, "Thin-Layer Approximation and Algebraic Model for Separated Turbulent Flows," AIAA Paper No. 78-257, 1978.

11. J. L. Steger, C. J. Nietubicz, and K. R. Heavey, "A General Curvilinear Grid Generation Program for Projectile Configurations," U.S. Army Ballistic Research Laboratory, Aberdeen Proving Ground, Maryland, ARBRL-MR-03142, October 1981. (AD A107334)

12. L. D. Kayser, "Experimental Study of Separation from the Base of a Cone at Supersonic Speeds," U.S. Army Ballistic Research Laboratory, Aberdeen Proving Ground, Maryland, BRL Report No. 1737, August 1974. (AD A005015)

LIST OF SYMBOLS

a	speed of sound
a_∞	free stream speed of sound
A	cross sectional area at the base
c_p	specific heat at constant pressure
C_p	pressure coefficient, $2(p - p_\infty)/\rho_\infty u_\infty^2$
D	body diameter (57.15mm)
e	total energy per unit volume/$\rho_\infty a_\infty^2$
$\hat{q}$	vector of dependent variables
$\hat{E}$, $\hat{F}$	flux vector of transformed Navier-Stokes equations
$\hat{H}$	η-invariant source vector
I	identity matrix
J	Jacobian of transformation
M	Mach number
M_∞	free stream Mach number
p	pressure/$\rho_\infty a_\infty^2$
p_∞	free stream pressure
Pr	Prandtl number, $\mu_\infty c_p/\kappa_\infty$
R	body radius
Re	Reynolds number, $\rho_\infty a_\infty D/\mu_\infty$
$\hat{S}$	viscous flux vector
t	physical time
u,v,w	Cartesian velocity components/a_∞
u_∞	free stream velocity
U,V,W	Contravariant velocity components/a_∞
x,y,z	physical Cartesian coordinates
α	angle of attack

γ	ratio of specific heats
κ	coefficient of thermal conductivity/κ_∞
κ_∞	coefficient of thermal conductivity at free stream conditions
μ	coefficient of viscosity/μ_∞
μ_∞	coefficient of viscosity at free stream conditions
ξ,η,ζ	transformed coordinates in axial, circumferential and radial directions
ρ	density/ρ_∞
ρ_∞	free stream density
τ	transformed time
ϕ	circumferential angle

Superscript

*	critical value

Subscript

b	base

DISTRIBUTION LIST

No. of Copies	Organization
12	Administrator Defense Technical Info Center ATTN: DTIC-DDA Cameron Station Alexandria, VA 22314
1	Commander US Army Materiel Command ATTN: AMCDRA-ST 5001 Eisenhower Avenue Alexandria, VA 22333
7	Commander Armament R&D Center US Army AMCCOM ATTN: SMCAR-TDC SMCAR-TSS SMCAR-LCA-F Mr. D. Mertz Mr. A. Loeb Mr. S. Wasserman Mr. H. Hudgins Mr. E. Friedman Dover, NJ 07801
1	Commander US Army Armament, Munitions and Chemical Command ATTN: AMSMC-LEP-L Rock Island, IL 61299
1	Director Benet Weapons Laboratory Armament R&D Center US Army AMCCOM ATTN: SMCAR-LCB-TL Watervliet, NY 12189
1	Commander US Army Aviation Research and Development Command ATTN: AMSAV -E 4300 Goodfellow Blvd. St. Louis, MO 63120
1	Commander US Army Missile Command ATTN: AMSMI-R Redstone Arsenal, AL 35898

No. of Copies	Organization
1	Director US Army Air Mobility Research and Development Laboratory Ames Research Center Moffett Field, CA 94035
1	Commander US Army Communications Research and Development Command ATTN: AMSEL-ATDD Fort Monmouth, NJ 07703
1	Commander US Army Electronics Research and Development Command Technical Support Activity ATTN: AMDSD-L Fort Monmouth, NJ 07703
2	Commander US Army Missile Command ATTN: AMSMI-RDK Dr. B. Walker Mr. R. Deep Redstone Arsenal, AL 35898
1	Commander US Army Missile Command ATTN: AMSMI-YDL Redstone Arsenal, AL 35898
1	Commander US Army Tank Automotive Command ATTN: AMSTA-TSL Warren, MI 48090
1	Director US Army TRADOC Systems Analysis Activity ATTN: ATAA-SL White Sands Missile Range, NM 88002
1	Commander US Army Research Office P. O. Box 12211 Research Triangle Park, NC 27709

DISTRIBUTION LIST

No. of Copies	Organization
1	Commander US Naval Air Systems Command ATTN: AIR-604 Washington, D. C. 20360
1	Commander US Naval Surface Weapons Center ATTN: Code DK20 Dahlgren, VA 22448
2	Commander US Naval Surface Weapons Center ATTN: Code 312 Mr. R. Voisinet Code R44 Dr. T. Zien Silver Spring, MD 20910
1	Commander US Naval Weapons Center ATTN: Code 3433 Tech Lib China Lake, CA 93555
1	Director NASA Langley Research Center ATTN: NS-185, Tech Lib Langley Station Hampton, VA 23365
3	Director NASA Ames Research Center ATTN: MS-202A-14, Dr. P. Kutler MS-202-1, Dr. T. Pulliam MS-227-8, Dr. L. Schiff Moffett Field, CA 94035
2	Commandant US Army Infantry School ATTN: ATSH-CD-CSO-OR Fort Benning, GA 31905
1	Sandia National Laboratory ATTN: Division No. 1331, Mr. H.R. Vaughn P.O. Box 580 Albuquerque, NJ 87115
1	HQDA DAMA-ART-M Washington, DC 20310
1	AFWL/SUL Kirtland AFB, NM 87117
1	Stanford University Department of Aeronautics and Astronautics ATTN: Prof. J. Steger Stanford, CA 94305
1	University of California, Davis Department of Mechanical Engineering ATTN: Prof. H.A. Dwyer Davis, CA 95616
1	University of Delaware Mechanical and Aerospace Engineering Department ATTN: Dr. J. E. Danberg Newark, DE 19711
1	University of Florida Dept. of Engineering Sciences College of Engineering ATTN: Prof. C. C. Hsu Gainesville, FL 32601
1	University of Illinois at Urbana Champaign Department of Mechanical and Industrial Engineering ATTN: Prof. W. L. Chow Urbana, IL 61801
1	University of Maryland Dept. of Aerospace Engr ATTN: Dr. J. D. Anderson, Jr. College Park, MD 20740
1	Commander US Army Development & Employment Agency ATTN: MODE-TED-SAB Fort Lewis, WA 98433

DISTRIBUTION LIST

No. of Copies	Organization
1	University of Notre Dame Department of Aeronautical and Mechanical Engineering ATTN: Prof. T. J. Mueller Notre Dame, IN 46556
1	University of Texas-Austin Department of Aerospace Engineering ATTN: Dr. J. J. Bertin Austin, TX 78712

Aberdeen Proving Ground

Dir, USAMSAA
ATTN: AMXSY -D
AMXSY -MP, H. Cohen

Cdr, USATECOM
ATTN: AMSTE -TO-F

Cdr, CRDC, AMCCOM
ATTN: SMCCR-RSP-A
SMCCR-MU
SMCCR-SPS-IL

END

FILMED

1-85

DTIC